

## Impact Dynamics for Elastic Membranes

Laurent Courbin,<sup>1</sup> Antonin Marchand,<sup>1</sup> Ashkan Vaziri,<sup>1</sup> Armand Ajdari,<sup>1,2</sup> and Howard A. Stone<sup>1,\*</sup>

<sup>1</sup>*Division of Engineering and Applied Sciences, Harvard University, Cambridge, Massachusetts 02138, USA*

<sup>2</sup>*Laboratoire Théorie et Microfluidique, UMR 7083 CNRS-ESPCI, 10 rue Vauquelin, 75005 Paris, France*

(Received 26 June 2006; published 15 December 2006)

We study the dynamic response of stretched thin polymeric films following an impact by a rigid sphere. We vary the sphere radius, the impact velocity, and the film tension, and measure the contact time and the maximum deflection of the film during the impact. The response is sensitive to nonlinearities associated with the additional tension provided by the deformation. A physical model at the scaling level is presented. This allows us (i) to understand qualitatively experimental and numerical results and (ii) to present a diagram mapping different possible impact dynamics for membrane systems, which accounts for the interplay between membrane tension, intrinsic modulus, and geometrical factors such as the frame size and the sphere radius.

DOI: 10.1103/PhysRevLett.97.244301

PACS numbers: 45.50.Tn, 46.70.Hg, 62.20.-x

Understanding the impact dynamics of two colliding solids or an object with a stationary surface is of importance for diverse phenomena such as the mechanics of shaken granular materials [1], the energy mitigating effects of foams on projectiles and explosions [2], sporting events such as trampolines and various ball games [3], ordinary model problems involving bouncing (e.g., as a qualitative characterization of materials), and even particle collisions involved in cosmic radiation [4]. Basic descriptions all start with the pioneering Hertz contact problem, which is based on linear elasticity [5]. Inelastic effects, such as viscoelastic dissipation [6] and plastic deformation [7–9], have been reported to occur during the impact. Some of the initial kinetic energy can also be radiated into the substrate as elastic waves [10,11] or stored in vibration modes such as bending [12]. Possible end effects have also been reported when the target substrate is surrounded by walls [13].

The best known example of this type of problem is the Hertzian quasistatic collision between a rigid sphere and a thick elastic plate [14]. At low velocity of impact, the response is given by comparing the initial kinetic energy of the impacting sphere with the potential energy of elastic deformation. Such an energy balance leads to scaling relations for both the variations of the maximum deformation and the contact time of the impact. Extensions of this work have mainly considered impact with finite thickness plates [7,11–13] and indentation of clamped films [15]. Moreover, one significant complication in analyzing a problem in this class is that nonlinearities between the states of strain and stress arise as a consequence of finite deformation.

Here we examine the dynamics of impact of a rigid sphere with a thin elastic sheet: finite deformation produces significant variations of the mean stress in the sheet and these nonlinearities affect the details of the response. We examine this problem via extensive experiments, a set of numerical simulations, and physical arguments that lead to scaling relationships, which capture the most significant

aspects of our measurements, and provide a “map” of the dynamical response for the various physical limits.

*Experiments.*—An elastic membrane is clamped between two large Plexiglas annular disks with inner and outer diameters, respectively, 190.5 and 266.7 mm. Care is taken to avoid any initial pretension in the membrane before placing it on a lubricated cylindrical frame with inner and outer diameters, respectively, 95.3 and 114.3 mm [see the experimental setup in Fig. 1(a)]. This circular frame, with radius  $R_F = 52.4$  mm, allows the application of a uniform tension to the membrane, which prevents the formation of wrinkling observed when an elastic sheet is submitted to a uniaxial tensile strain [16]. Furthermore, the frame thickness (9.5 mm) is large enough to ensure the membrane supports the applied load. The mass of the clamping system,  $M_{\text{clamp}} = 390$  g, sets the value of the initial background stress in the membrane:  $\sigma_b \sim M_{\text{clamp}}g/2\pi R_F h_f$ , where  $h_f$  is the film thickness. Further, we can tune the background stress by the addition of annular brass disks placed on the initial annular disks so that  $2.7 \text{ MPa} < \sigma_b < 7.3 \text{ MPa}$ .

By measuring the deformation of the membrane for a given background stress, we estimate the Young’s modulus of the elastic membrane, while a profilometer (Tencor Instruments, a-Step 2000) is used to determine its thickness. We use two different materials, namely, Saran Wrap (Johnson) and Mylar-A films (Polymer Plastics Corporation). The Saran Wrap is a common stretchable film of low Young’s modulus ( $E_f \approx 250$  MPa) with thickness  $h_f = 10 \mu\text{m}$  and density  $\rho_f = 1.68 \text{ g/cm}^3$ . The Young’s modulus of the Mylar-A is higher,  $E_f \approx 2.5$  GPa, with thickness  $h_f = 25 \mu\text{m}$  and density  $\rho_f = 1.19 \text{ g/cm}^3$ . The spheres used as impacting objects are made of magnetizable stainless steel:  $E_S \approx 200$  GPa and  $\rho_S = 7.8 \text{ g/cm}^3$ . A custom-made electromagnet allows us to trigger the release of the sphere from a specific height,  $H_0$ , above the membrane [see Fig. 1(a)]. By tuning  $H_0$  we control the sphere velocity measured at the onset of the

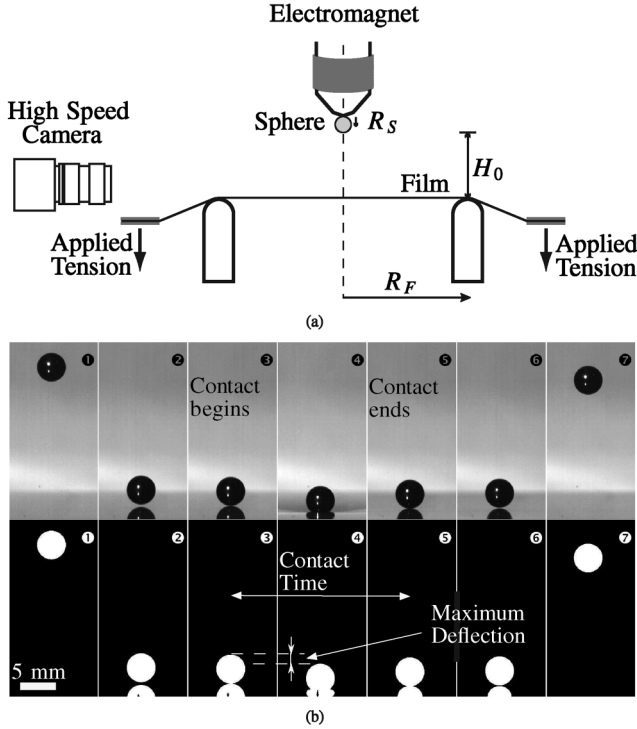


FIG. 1. (a) Schematic of the experimental setup. (b) Position of the sphere bouncing off Saran Wrap. The top and the bottom series of images are, respectively, frames from the original movie and the processed images. The corresponding times are as follows: (1)  $t = 15$  ms, (2)  $t = 43.75$  ms, (3)  $t = 44$  ms, (4)  $t = 46.5$  ms, (5)  $t = 49$  ms, (6)  $t = 49.25$  ms, and (7)  $t = 103.25$  ms. The origin of time is taken once the bottom of the sphere appears in the frame. The release height and sphere radius are  $H_0 = 27$  mm and  $R_S = 2$  mm. The values of the contact time and the maximum amplitude of deflection of the sheet during the impact are, respectively,  $\tau = 5$  ms and  $\delta = 1.24$  mm.

impact,  $V_i$ , in the range 0.1–1 m/s. The sphere radius,  $R_S$ , changes from 0.35 to 3.5 mm; thus their mass  $M_S = \rho_S \frac{4\pi}{3} R_S^3$  varies in the range  $1.38 \times 10^{-3}$ –1.38 g. The position of the sphere as a function of time is recorded with a high-speed camera (Phantom V5) working at a frame rate 1000–10 000 frames/s.

The two primary outputs of our measurements are the maximum deflection of the elastic sheet,  $\delta$ , and the contact time,  $\tau$ , which are obtained by analyzing the high-speed images with a custom-made software written with MATLAB. Figure 1(b) shows the evolution of the position of the sphere during the impact on Saran Wrap. The reflection of the sphere prior to impact with the membrane allows us to precisely define the beginning and end of the contact [see the processed images in Fig. 1(b)]. Furthermore, numerical simulations of this system, using the finite-element software ABAQUS, allow us to vary both the background stress and the speed of impact across several orders of magnitude and thus to obtain more insight into the variations of  $\delta$  and  $\tau$  with  $\sigma_b$  and  $V_i$ . The numerical simulations

were carried out for  $R_F = 52.4$  mm and  $R_F = 104.8$  mm to study the effect of the frame size.

**Results.**—Having performed the image analysis, we obtain for a given background stress and material the variations of  $\tau$  and  $\delta$  with the impact speed of the sphere (see Fig. 2). As depicted in this figure, the contact time,  $\tau$ , which is of the order of a few ms, is strongly dependent on the sphere radius but is a weak function of  $V_i$ , whereas the maximum deflection of the membrane,  $\delta$ , is strongly dependent on both  $V_i$  and  $R_S$  [see Fig. 2(b)]. Moreover, our experiments show that the ratio  $\delta/\tau V_i = \beta$  is approximately constant with  $\beta \approx \frac{1}{4}$  as expected for a parabolic evolution of the deflection with time during the impact [17] (see the inset of Fig. 2). As a result, the variations of the contact time,  $\tau \sim \delta/V_i$ , can be obtained straightforwardly from those of the maximum deflection,  $\delta$ . We obtain similar dependencies for the two materials and background

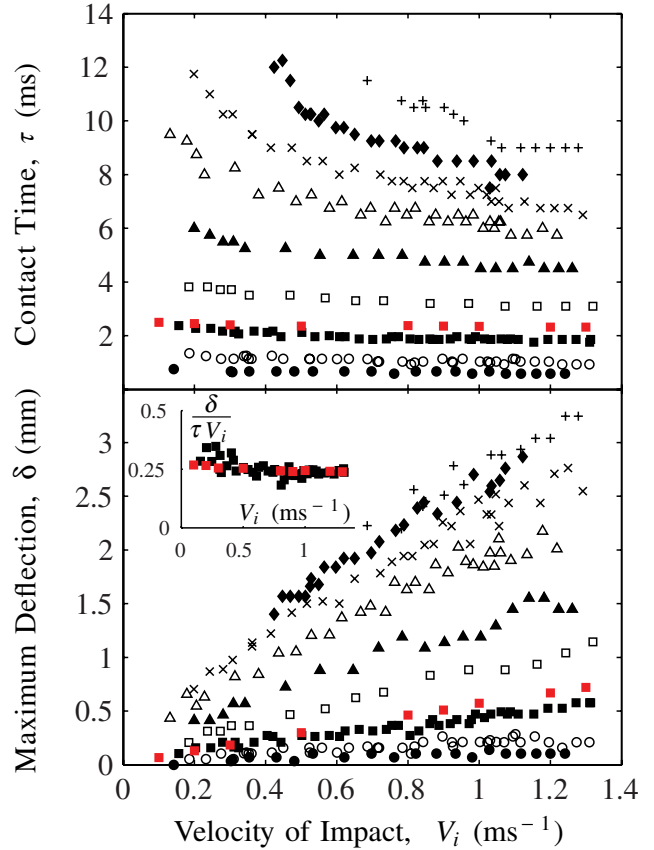


FIG. 2 (color online). Top panel: Variation of the contact time  $\tau$  with the velocity of impact  $V_i$ . Bottom panel: Evolution of the maximum deflection of the membrane  $\delta$  with  $V_i$ . Inset: Dependence of the ratio  $\frac{\delta}{\tau V_i}$  with  $V_i$ . The different symbols correspond to experiments on Saran Wrap for different values of the sphere radius: ( $\bullet$ )  $R_S = 0.35$  mm, ( $\circ$ )  $R_S = 0.5$  mm, ( $\blacksquare$ )  $R_S = 0.795$  mm, ( $\square$ )  $R_S = 1.25$  mm, ( $\blacktriangle$ )  $R_S = 1.75$  mm, ( $\triangle$ )  $R_S = 2.38$  mm, ( $\times$ )  $R_S = 2.78$  mm, ( $\blacklozenge$ )  $R_S = 3$  mm, and ( $+$ )  $R_S = 3.175$  mm. A set of numerical data for  $R_S = 0.795$  mm is provided for comparison (red solid squares).

stresses (in total, more than 600 experiments were analyzed) as well as in the numerical simulations. We next rationalize these observations in terms of the variations of the maximum deflection.

*Discussion.*—We begin to understand our results by simply comparing the initial kinetic energy of the sphere,  $E_k = \frac{1}{2}M_S V_i^2$ , with an estimate of the energy stored in the membrane during the impact,  $E_e^m$ . Two distinct parameters contribute to the elasticity of the membrane: the applied background stress,  $\sigma_b$ , and the intrinsic modulus of the membrane,  $E_f$ . As nonlinearities have to be taken into account at the scaling level, we then expect the elastic energy in the membrane to be  $E_e^m \approx \sigma_b h_f \ell^2 (\frac{\delta}{\ell})^2 + E_f h_f \ell^2 (\frac{\delta}{\ell})^4$ , where  $\ell$  is the typical length over which the membrane is deformed and the strain is  $\mathcal{O}(\frac{\delta}{\ell})^2$ . Moreover, due to the vibrations of the membrane during the impact, there is kinetic energy,  $E_k^m$ , in the elastic sheet:  $E_k^m \approx \rho_f h_f \ell^2 (\frac{\delta}{\tau})^2$ . The total energy for this system is  $E_k \approx E_e^m + E_k^m$ . Assuming that the frame size is infinite ( $\ell \ll R_F$ ) and that elastic and kinetic energies are of the same order of magnitude, we determine two possible values for the typical length  $\ell$ :  $\ell = \ell_1 = \sqrt{\sigma_b / \rho_f \tau}$  or  $\ell = \ell_2 = (\sqrt{E_f / \rho_f \tau} \delta)^{1/2}$ . When  $\ell_1 > \ell_2$  (i.e., when  $\delta / \tau \approx V_i < V^*$ , with  $V^* = \frac{\sigma_b}{\sqrt{E_f \rho_f}}$ ), the elastic response is controlled by the background stress,  $\sigma_b$ , otherwise ( $\ell_2 > \ell_1$ , or  $V_i > V^*$ ) by the Young's modulus,  $E_f$ . For Saran Wrap, the characteristic lengths  $\ell_1$  and  $\ell_2$  vary, respectively, in the ranges 20–500 and 5–90 mm, whereas the frame radius is  $R_F = 52.4$  mm. Consequently, the finite nature of the frame size has to be taken into account in our model: when  $\ell_1 > R_F$  or  $\ell_2 > R_F$ , the typical length  $\ell$  to be used in estimating the energy stored in the membrane is  $\ell = R_F$ .

This physical analysis allows us to construct a map of the possible regimes of impact dynamics for membrane systems (see Fig. 3). This diagram is presented in terms of two dimensionless parameters,  $V_i/V^*$  and  $M_S/M^*$ , with  $M^* = R_F^2 h_f \rho_f$ , and clearly depicts the complexity of the response of impact in elastic membranes. Indeed, depending on the respective values of  $V_i/V^*$  and  $M_S/M^*$ , four different regimes can be identified: the elastic response can be controlled by  $\sigma_b$  (regimes I and II) or by  $E_f$  (regimes III and IV); also, the wavelike perturbation to the membrane does not reach the boundaries (regimes I and III) or is limited by the frame size (regimes II and IV). Moreover, using the relation  $\tau \sim \delta/V_i$ , we determine a number of scaling laws for the evolutions of both  $\delta$  and  $\tau$  in each regime (see Fig. 3); however, checking the validity of these scaling laws is difficult since many data are in the vicinity of boundaries between the different regions. For Saran Wrap and  $\sigma_b = 2.7$  MPa,  $V^*$ , which defines the transition between regimes I to III, is of the order of  $V^* \approx 4$  m/s and is out of the range of our experimental conditions. Moreover, a large fraction of sphere radii are above the

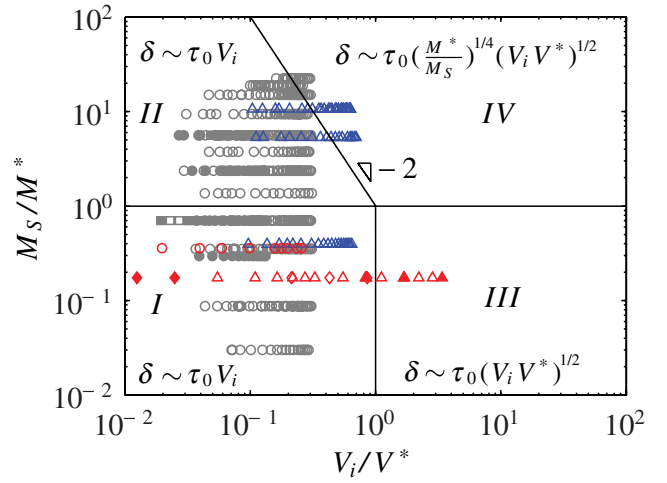


FIG. 3 (color online). Diagram mapping the impact dynamics in the membrane as a function of the dimensionless parameters  $V_i/V^*$  and  $M_S/M^*$ , where  $V^* = \frac{\sigma_b}{\sqrt{E_f \rho_f}}$  and  $M^* = R_F^2 h_f \rho_f$ . Also, in this figure we use  $\tau_0 = \sqrt{\frac{M_S}{\sigma_b h_f}}$ . The colors stand for different material and the numerical simulations: black (Saran Wrap), blue (Mylar-A), and red numerical results. The different symbols correspond to different values of the background tension: ( $\blacktriangle$ )  $\sigma_b = 0.53$  MPa, ( $\diamond$ )  $\sigma_b = 2.1$  MPa, ( $\circ$ )  $\sigma_b = 2.7$  MPa, ( $\triangle$ )  $\sigma_b = 3.3$  MPa, ( $\bullet$ )  $\sigma_b = 5.2$  MPa, ( $\square$ )  $\sigma_b = 6.4$  MPa, ( $\blacklozenge$ )  $\sigma_b = 7.2$  MPa, and ( $\blacksquare$ )  $\sigma_b = 7.3$  MPa.

critical sphere radius,  $R_S^* \approx 1.1$  mm, obtained by the estimate of  $M^*$ , which sets transitions I-II and III-IV. Consequently, our experimental results mostly cover region II, in which the elasticity is controlled by the imposed background stress and the frame size is important (see Fig. 3). We will explore in a future communication regimes III and IV using numerical simulations that are not subjected to the limitations imposed by plasticity [17].

To validate our model, we next compare the initial kinetic energy of the sphere,  $E_k$ , with an estimation of the energy of deformation of the membrane:

$$E_e^{m(0)} = c_1 \sigma_b h_f \ell^2 \left(\frac{\delta}{\ell}\right)^2 + c_2 E_f h_f \ell^2 \left(\frac{\delta}{\ell}\right)^4, \quad (1)$$

where  $c_1$  and  $c_2$  are two numerical constants and  $\ell$  is defined as above:  $\ell = \min\{\max\{\ell_1, \ell_2\}, R_F\}$ . When  $c_1 = c_2 = 1$ , this first estimate allows us to obtain good qualitative agreement with both numerical and experimental results since the energy balance partially collapses data onto a single curve (not shown here); however, a significant scatter is still observed for large  $V_i$ , small  $\sigma_b$  and between points obtained for the two values of  $R_F$ . We therefore need a more sophisticated model. The origin of the additional variability is in part related to logarithmic corrections characteristic of two-dimensional elasticity that slightly modify the scaling relations defining the evolutions of  $\delta$  in regimes I and II.

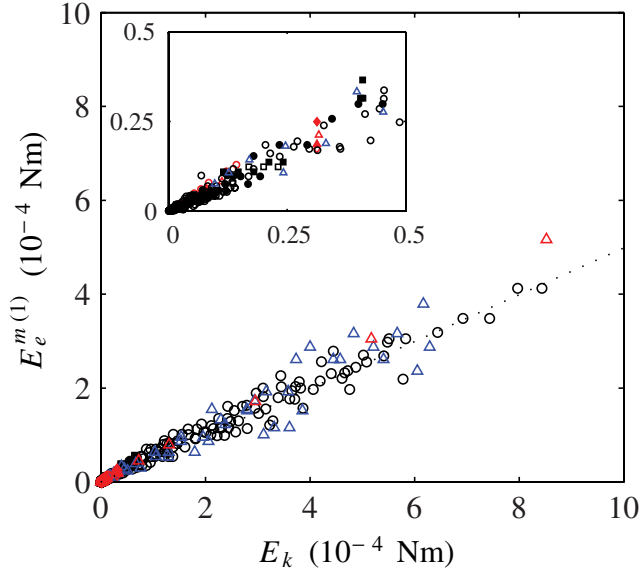


FIG. 4 (color online). Evolution of the stored energy in the membrane obtained with the calculation of elastic energy of a membrane submitted to a deformation  $\delta$  located at its center,  $E_e^{m(1)}$ , as a function of the initial kinetic energy of the impacting sphere,  $E_k$ . Inset: Magnification at low energies. The different symbols and colors are identical to those in Fig. 3. The dotted line is a guide for the eyes and has a slope of  $1/2$ .

In order to get a better evaluation of the elastic energy of the elastic sheet,  $E_e^m$ , we next calculate the familiar elastic energy of a membrane submitted to a deformation  $\delta$  located at its center,  $E_e^m = \frac{h_f \sigma_b}{2} \int dS (\nabla u)^2$ , where the integration is over the surface of the membrane, and  $u(\vec{r})$  is the induced displacement of the interface from its equilibrium position [18]. Details of the calculation will be presented elsewhere [17]. This calculation allows us to correct the first estimate of the stored energy in the membrane,  $E_e^{m(0)}$ , and to add a logarithmic decay for the displacement in the new estimation of this energy,  $E_e^{m(1)}$ ; one finally finds

$$E_e^{m(1)} = \frac{\pi}{\ln\left(\frac{\ell}{\sqrt{\delta R_S}}\right)} \sigma_b h_f \ell^2 \left(\frac{\delta}{\ell}\right)^2 + c_2 E_f h_f \ell^2 \left(\frac{\delta}{\ell}\right)^4, \quad (2)$$

where  $\ell$  is defined as above. Depending on experimental conditions, the value of  $\frac{\pi}{\ln(\ell/\sqrt{\delta R_S})}$  varies in the range (0.5–1.5) and is significant since it accounts for geometrical variables,  $R_S$  and  $\ell$ . Because of a lack of a full nonlinear elasticity computation, we take  $c_2 = 1$  to plot in Fig. 4 the approximation of the stored energy given by Eq. (2),  $E_e^{m(1)}$ , as a function of the initial kinetic energy of the sphere,  $E_k$ . As shown in this figure, a strong correlation is found for both our experimental and numerical results (i.e., different values of  $V_i$ ,  $R_S$ ,  $\sigma_b$ ,  $E_f$ ,  $h_f$ , and  $R_F$ ): our physical model collapses much of the data onto a single curve.

As a final comment, let us note that our results suggest a variation close to  $E_e^{m(1)} \approx \frac{1}{2} E_k$  (see Fig. 4). As a consequence, roughly half of the initial kinetic energy has been stored in the membrane, the remaining part being dissipated in the vibrations of the film. It is worth noticing that this result is consistent with our physical model, which is based on the assumption that kinetic and elastic energies are of the same order of magnitude.

Characterizing the impact dynamics for model membrane systems is challenging since (i) it is experimentally difficult to study the response far from the boundaries of the diagram we presented above without other mechanisms coming into play, such as plasticity, and (ii) as we show in this Letter, nonlinearities play an important role. However, we believe that the general diagram presented in Fig. 3 provides a simple and robust way to understand, for a given situation, which parameters (frame size, membrane tension, etc.) control the impact dynamics. As a result, for any application, these are the parameters that should be tuned to modify significantly the impact characteristics.

The authors thank J. Vlassak and J. W. Hutchinson for helpful conversations. We thank the Harvard MRSEC (DMR-0213805) for partial support of this research.

\*Electronic address: has@deas.harvard.edu

- [1] A. Mehta and J. M. Luck, Phys. Rev. Lett. **65**, 393 (1990).
- [2] C. J. Clark and E. M. Bennet, U.S. Patent No. 4,589,341 (1986).
- [3] A. M. Nathan, D. A. Russell, and L. V. Smith, Engineering of Sport **5**, 2, 38 (2004).
- [4] E. Fermi, Phys. Rev. **75**, 1169 (1949).
- [5] H. Hertz, in *Miscellaneous Papers* (Macmillan, London, 1896), p. 146.
- [6] G. Kuwabara and K. Kono, Jpn. J. Appl. Phys. **26**, 1230 (1987).
- [7] C. V. Raman, Phys. Rev. **12**, 442 (1918).
- [8] W. Goldsmith, *Impact* (Arnold, London, 1960).
- [9] D. Tabor, Proc. R. Soc. A **192**, 247 (1948).
- [10] S. C. Hunter, J. Mech. Phys. Solids **5**, 162 (1957); J. Reed, J. Phys. D **18**, 2329 (1985).
- [11] J. P. A. Tillet, Proc. Phys. Soc. London, Sect. B **67**, 677 (1954).
- [12] C. Zener, Phys. Rev. **59**, 669 (1941).
- [13] R. Sondergaard, K. Chaney, and C. E. Brennen, J. Appl. Mech. **112**, 694 (1990).
- [14] A. E. H. Love, *A Treatise on the Mathematical Theory of Elasticity* (Cambridge University Press, Cambridge, 1944).
- [15] U. Komaragiri, M. R. Begley, and J. G. Simmonds, J. Appl. Mech. **72**, 203 (2005), and references therein.
- [16] E. Cerda, K. Ravi-Chandar, and L. Mahadevan, Nature (London) **419**, 579 (2002).
- [17] L. Courbin, A. Marchand, A. Vaziri, A. Ajdari, and H. A. Stone (to be published).
- [18] L. D. Landau and E. M. Lifshitz, *Theory of Elasticity* (Pergamon Press, Oxford, 1986).